Vol 15 No 7, July 2006
1009-1963/2006/15(07)/1502-09

Chinese Physics

© 2006 Chin. Phys. Soc.
and IOP Publishing Ltd

Theoretical simulations of emission spectra of Fe^{7+} and Fe^{8+}*

Zeng Jiao-Long(曾交龙)[a)b)†], Wang Yan-Gui(王雁桂)[b)],
Zhao Gang(赵 刚)[a)], and Yuan Jian-Min(袁建民)[a)b)]

[a)] *National Astronomical Observatories, Chinese Academy of Sciences, Beijing* 100012, *China*

[b)] *Department of Applied Physics, National University of Defense Technology, Changsha* 410073, *China*

(Received 13 June 2005; revised manuscript received 3 April 2006)

The energy levels, oscillator strengths, spontaneous radiative decay rates, and electron impact collision strengths are calculated for Fe VIII and Fe IX using the recently developed flexible atomic code (FAC). These atomic data are used to analyse the emission spectra of both laboratory and astrophysical plasmas. The *n*f–3d emission lines have been simulated for Fe VIII and Fe IX in a wavelength range of 6–14 nm. For Fe VIII, the predicted relative intensities of lines are insensitive to temperature. For Fe IX, however, the intensity ratios are very sensitive to temperature, implying that the information of temperature in the experiment can be inferred. Detailed line analyses have also been carried out in a wavelength range of 60–80 nm for Fe VIII, where the solar ultraviolet measurements of emitted radiation spectrometer records a large number of spectra. More lines can be identified with the aid of present atomic data. A complete dataset is available electronically from http://www.astrnomy.csdb.cn/EIE/.

Keywords: emission spectrum, Fe VIII and Fe IX, electron impact excitation
PACC: 3270, 3450, 3480

1. Introduction

There has long been interest in emission spectra of different ionization stages of iron ions. The iron project[1] has the main goal of computing on a large scale electron excitation cross sections and rates, which are of astrophysical and technological importance, for the iron-group elements. A large amount of atomic data has been obtained using the close-coupling scheme implemented by the *R*-matrix method. These atomic data are generally limited to energy levels with principle quantum number $n \leq 5$. Recently, Lepson *et al* [2] measured the emission lines of Fe VII–Fe X in an extreme ultraviolet range of 6–14 nm. The spectra were recorded at an electron density of $\sim 5\times10^{11}$ cm^{-3}. Spectral lines were observed for transition type of *n*f→3d with principle quantum number n as high as 9 or more for these iron ions. On the other hand, with the launch of new generation of x ray satellites (Chandra, XMM-Newton, etc.), more and more high resolution and high signal-to-noise ratio spectra of the astrophysical objects are available. Many absorption or emission lines from the L-shell transitions of iron ions belonging to different ionization stages including Fe^{7+} and Fe^{8+} have been observed in astrophysical objects.[3–5] Some work has been carried out to deal with the photoexcitation or autoionizing states.[6–9] To interpret the observed spectra, it is necessary to extend the atomic data to energy levels of higher principle quantum numbers.

An accurate and complete spectral model is essential to analyse and identify the lines from both the laboratory and astrophysical plasmas. For a complete model, one needs a large amount of atomic data, such as the energy levels, spontaneous radiative decay rates and electron impact collision strengths. For Fe VIII and Fe IX, extensive work has been devoted to the energy levels and oscillator strengths. Take Fe VIII as an example. A few studies were carried out in the Coulomb–Born[10,11] and distorted wave[12] approximations. Saraph *et al* [13] and Lynas-Gray *et al* [14] carried out comprehensive *ab initio* calculations to obtain the radiative data in the close-coupling approximation implemented by the *R*-matrix method. The last two studies are part of the opacity project.[15] Tiwary *et al* [16–18] calculated the excitation energies and oscillator strengths for transitions of $3s^23p^63d^2D \rightarrow 3s^23p^53d^2\ {}^2P^0$, ${}^2D^0$ and ${}^2F^0$ using the CIV3 program of Hibbert[19] or the multi-configuration Hartree–Fock (MCHF) method.[20] All these calculations were carried out in an LS coupling scheme. Fawcett[21] calculated the oscillator strengths

*Project supported by the National Natural Science Foundation of China (Grant Nos 10204024, 10373014, 10433010 and 10474138).
†E-mail: jiaolongzeng@hotmail.com

and wavelengths for some lines using an intermediate coupling scheme.

Bhatia and Eissner[22] computed the collision strengths for 73 fine structure energy levels belonging to the configurations of $3s^23p^63d$, $3s^23p^53d^2$, $3s^23p^64s$, $3s^23p^64p$, and $3s^23p^53d4s$ of Fe VIII. The calculation was carried out in the distorted wave approximation using the superstructure program.[23] Griffin *et al* [24] calculated the electron impact excitation cross sections of Fe VIII using the R-matrix close-coupling theory. In addition to the configurations that Bhatia and Eissner[22] had investigated, Griffin *et al* [24] considered further configurations of $3s^23p^64d$ and $3s^23p^64f$ in their calculation. For the electron impact excitation of Fe IX, Storey *et al* [25] calculated the collision strengths and thermally averaged collision strengths between the 140 energetically lowest levels as part of the iron project. Their calculation had been carried out in the close-coupling approximation implemented by the R-matrix method. The inclusion of more resonances led to a great increase in the excitation rate among the levels of $3s^23p^53d$ configuration as compared with previous work.[26−28]

The present paper first calculates the electron impact collision strengths for Fe VIII and Fe IX, and then simulates the emission spectra. Extensive configuration interactions including configurations such as $3s^23p^6nl$, (n=6,7,8,9; l=1, 3) for Fe VIII and $3s^23p^5nl$, (n=6,7; l=2,3) for Fe IX have been considered in the calculation of collision strengths. The effective collision strengths are obtained by averaging the collision strengths over the Maxwellian electron velocity distribution. The energy levels, spontaneous radiative decay rates and effective collision strengths are used to solve the statistical equilibrium equations for the level populations. Once the level populations have been obtained, one can use them to analyse and interpret spectra of both the laboratory and astrophysical plasmas.

2. Atomic data

The calculating of the atomic structure and electron impact excitation has been carried out using the flexible atomic code (FAC) developed by Gu.[29] A fully relativistic approach based on the Dirac equation is used throughout the package. In the calculation of atomic structure, the energy levels of an atomic ion with N electrons are obtained by diagonalizing the relativistic Hamiltonian H (in atomic units):

$$H = \sum_{i}^{N}(c\boldsymbol{\alpha}\cdot\boldsymbol{P}_i + (\beta-1))c^2 + V_{\rm nuc}(r_i) + \sum_{i<j}^{n}\frac{1}{r_{ij}}, \quad (1)$$

where c is the speed of light in vacuum, $V_{\rm nuc}(r_i)$ is the potential due to the nucleus.

An atomic state is approximated by a linear combination of configuration state functions with the same symmetry

$$\Phi_\alpha(J\pi) = \sum_{i}^{n_{\rm c}} a_i(\alpha)\phi_\alpha^{(i)}(J\pi), \quad (2)$$

where $\phi_\alpha^{(i)}$ is a configuration state function (CSF) that is constructed from one-electron orbitals, $n_{\rm c}$ is the number of CSF and $a_i(\alpha)$ denotes the representation of the atomic state in this basis. A CSF is antisymmetrized products of a common set of orthonormal orbitals which are optimized on the basis of the relativistic Hamiltonian. The radial orbitals are derived from a modified Dirac–Fock–Slater iteration on a fictitious mean configuration with fractional occupation numbers, representing the average electron cloud of the configurations included in the calculation. Once the configuration interaction wavefunctions have been obtained, the radiative transition rates can be calculated in the single multipole approximation with arbitrary ranks. In the present work, E1, E2, M1 and M2 transition data are obtained and included in the statistical equilibrium.

The electron impact excitation cross section is calculated in the relativistic distorted wave approximation. Special attention is paid to the long-range contributions to the continuum-continuum radial integral by using the phase–amplitude method for the continuum wavefunctions. The contributions from large angular momentum partial waves for the allowed transitions are taken into account in the Coulomb–Beth approximation. To ensure the convergence of the collision strengths, large angular momentum contributions (the maximum partial waves up to 50) are taken into account. Higher partial wave contributions have been included in the Coulomb–Bethe approximation.[30]

For Fe VIII, spontaneous radiative decay rates and electron impact collision strengths have been calculated for the 102 fine-structure levels belonging to the following configurations: ([Ne])$3s^23p^63d$, $3s^23p^53d^2$, $3s^23p^53d4s$, $3s^23p^64l$(l=0,1,2,3), $3s^23p^65l$ (l=0,1,2,3,4), $3s^23p^6nl$,(n=6,7,8,9; l=1,3). Interactions among these configurations are included in the

calculations of the atomic structure and electron impact excitation cross section. Table 1 lists the theoretical energy levels as well as the experimental values[31] wherever available. The experimental results for the configuration of $3s^2 3p^6 4d$ are taken from recent line identifications of Fe VIII carried out by Ekberg and Feldman.[32] Note that some levels of $3s^2 3p^5 3d^2$ are so strongly mixed that the level designations are just labels. Fairly good agreement is observed between the theoretical and experimental levels wherever available. Except for a few levels belonging to the configuration of $3s^2 3p^5 3d^2$, the relative difference is less than 1%.

Table 1. Calculated and measured[31] energy levels (in eV) for Fe VIII. A jj-coupling scheme is used for level designation. From the level 3, the relativistic orbital is omitted if it is full.

No.	Level designation	J	Theo.	Expt.[31]
1	$3p^6 3d_{3/2}$	3/2	0.000	
2	$3p^6 3d_{3/2}$	5/2	0.221	0.228
3	$3p^3_{3/2}(3d^2_{3/2})_2$	1/2	47.700	
4	$(3p^3_{3/2}3d_{3/2})_1 3d_{5/2}$	3/2	47.811	
5	$(3p^3_{3/2}3d_{3/2})_0 3d_{5/2}$	5/2	47.997	
6	$(3p^3_{3/2}3d_{3/2})_1 3d_{5/2}$	7/2	48.268	
7	$3p^3_{3/2}(3d^2_{5/2})_4$	11/2	50.461	
8	$(3p^3_{3/2}3d_{3/2})_3 3d_{5/2}$	9/2	50.679	
9	$3p^3_{3/2}(3d^2_{3/2})_2$	7/2	50.946	
10	$(3p^3_{3/2}3d_{3/2})_1 3d_{5/2}$	5/2	51.059	
11	$3p^3_{3/2}(3d^2_{3/2})_2$	5/2	51.232	
12	$(3p^3_{3/2}3d_{3/2})_3 3d_{5/2}$	3/2	51.449	
13	$(3p_{1/2}3d_{3/2})_2 3d_{5/2}$	1/2	51.738	
14	$4s_{1/2}$	1/2	52.058	
15	$3p^3_{3/2}(3d^2_{3/2})_2$	3/2	52.424	
16	$3p^3_{3/2}(3d^2_{3/2})_2$	5/2	52.575	
17	$3p^3_{3/2}(3d^2_{5/2})_4$	9/2	52.620	
18	$(3p^3_{3/2}3d_{3/2})_3 3d_{5/2}$	7/2	52.753	
19	$3p^3_{3/2}(3d^2_{5/2})_2$	5/2	53.171	53.468
20	$3p^3_{3/2}(3d^2_{5/2})_4$	5/2	53.219	
21	$3p^3_{3/2}(3d^2_{5/2})_2$	3/2	53.389	
22	$3p_{1/2}(3d^2_{5/2})_4$	7/2	53.658	53.878
23	$3p^3_{3/2}(3d^2_{5/2})_2$	1/2	54.348	
24	$(3p^3_{3/2}3d_{3/2})_3 3d_{5/2}$	11/2	55.064	
25	$3p_{1/2}(3d^2_{5/2})_2$	3/2	55.072	
26	$3p^3_{3/2}(3d^2_{5/2})_2$	7/2	55.334	
27	$(3p^3_{3/2}3d_{3/2})_3 3d_{5/2}$	7/2	55.693	55.503
28	$3p_{1/2}(3d^2_{5/2})_4$	9/2	56.049	
29	$(3p_{1/2}3d_{3/2})_2 3d_{5/2}$	9/2	56.367	
30	$3p_{1/2}(3d^2_{5/2})_2$	5/2	56.855	56.954
31	$3p^3_{3/2}(3d^2_{5/2})_2$	7/2	56.964	
32	$(3p^3_{3/2}3d_{3/2})_2 3d_{5/2}$	5/2	57.149	
33	$(3p_{1/2}3d_{3/2})_2 3d_{5/2}$	3/2	57.408	
34	$3p_{1/2}(3d^2_{3/2})_0$	1/2	57.665	
35	$(3p^3_{3/2}3d_{3/2})_3 3d_{5/2}$	3/2	59.660	
36	$3p_{1/2}(3d^2_{5/2})_2$	5/2	60.161	
37	$(3p^3_{3/2}3d_{3/2})_2 3d_{5/2}$	3/2	60.471	
38	$(3p^3_{3/2}3d_{3/2})_2 3d_{5/2}$	1/2	60.475	
39	$(3p^3_{3/2}3d_{3/2})_2 3d_{5/2}$	9/2	60.828	
40	$(3p_{1/2}3d_{3/2})_1 3d_{5/2}$	7/2	60.916	

continued Table 1

No.	Level designation	J	Theo.	Expt.[31]
41	$4p_{1/2}$	1/2	62.701	63.266
42	$4p_{3/2}$	3/2	62.997	63.920
43	$3p^3_{3/2}(3d^2_{5/2})_0$	3/2	64.039	63.048
44	$3p_{1/2}(3d^2_{5/2})_0$	1/2	65.222	64.574
45	$(3p^3_{3/2}3d_{3/2})_2 3d_{5/2}$	5/2	68.358	66.444
46	$(3p_{1/2}3d_{3/2})_2 3d_{5/2}$	7/2	69.096	67.169
47	$(3p^3_{3/2}3d_{3/2})_3 3d_{5/2}$	1/2	75.617	73.394
48	$3p^3_{3/2}(3d^2_{5/2})_2$	3/2	76.009	73.790
49	$3p^3_{3/2}(3d^2_{5/2})_4$	5/2	77.178	73.952
50	$3p_{1/2}(3d^2_{5/2})_2$	3/2	77.267	74.027
51	$4d_{3/2}$	3/2	81.140	81.051
52	$4d_{5/2}$	5/2	81.190	81.111
53	$4f_{5/2}$	5/2	94.301	94.687
54	$4f_{7/2}$	7/2	94.315	94.699
55	$5s_{1/2}$	1/2	95.669	
56	$5p_{1/2}$	1/2	100.286	
57	$5p_{3/2}$	3/2	100.487	
58	$(3p^3_{3/2}3d_{3/2})_0 4s_{1/2}$	1/2	101.653	
59	$(3p^3_{3/2}3d_{3/2})_1 4s_{1/2}$	3/2	101.968	
60	$(3p^3_{3/2}3d_{5/2})_2 4s_{1/2}$	5/2	102.556	
61	$(3p^3_{3/2}3d_{3/2})_2 4s_{1/2}$	1/2	103.394	103.857
62	$(3p^3_{3/2}3d_{5/2})_4 4s_{1/2}$	9/2	103.950	
63	$(3p^3_{3/2}3d_{5/2})_2 4s_{1/2}$	3/2	104.044	104.498
64	$(3p^3_{3/2}3d_{3/2})_3 4s_{1/2}$	7/2	104.265	105.033
65	$(3p^3_{3/2}3d_{3/2})_3 4s_{1/2}$	5/2	104.619	105.374
66	$3p_{1/2}3d_{3/2})_2 4s_{1/2}$	3/2	105.011	105.740
67	$(3p^3_{3/2}3d_{5/2})_4 4s_{1/2}$	7/2	105.471	106.000
68	$(3p^3_{3/2}3d_{3/2})_2 4s_{1/2}$	5/2	106.191	106.703
69	$(3p^3_{3/2}3d_{5/2})_3 4s_{1/2}$	7/2	108.038	108.450
70	$5d_{3/2}$	3/2	108.184	
71	$5d_{5/2}$	5/2	108.208	
72	$(3p^3_{3/2}3d_{5/2})_3 4s_{1/2}$	5/2	108.329	108.705
73	$(3p^3_{3/2}3d_{3/2})_2 4s_{1/2}$	3/2	108.471	108.793
74	$3p_{1/2}3d_{3/2})_1 4s_{1/2}$	1/2	108.578	108.891
75	$(3p^3_{3/2}3d_{5/2})_3 4s_{1/2}$	5/2	108.810	108.985
76	$(3p^3_{3/2}3d_{5/2})_2 4s_{1/2}$	3/2	109.092	109.273
77	$3p_{1/2}3d_{5/2})_2 4s_{1/2}$	5/2	109.299	109.643
78	$3p_{1/2}3d_{5/2})_3 4s_{1/2}$	7/2	109.571	110.014
79	$3p_{1/2}3d_{5/2})_2 4s_{1/2}$	3/2	110.039	110.236
80	$3p_{1/2}3d_{5/2})_3 4s_{1/2}$	5/2	110.166	110.451
81	$5f_{5/2}$	5/2	114.012	114.941
82	$5f_{7/2}$	7/2	114.017	114.946
83	$5g_{7/2}$	7/2	115.007	
84	$5g_{9/2}$	9/2	115.007	
85	$6p_{1/2}$	1/2	117.711	
86	$6p_{3/2}$	3/2	117.801	
87	$6f_{5/2}$	5/2	124.964	126.037
88	$6f_{7/2}$	7/2	124.966	126.038

continued Table 1

No.	Level designation	J	Theo.	Expt.[31]
89	$(3p^3_{3/2}3d_{5/2})_1 4s_{1/2}$	3/2	126.774	
90	$(3p^3_{3/2}3d_{5/2})_1 4s_{1/2}$	1/2	126.789	
91	$7p_{1/2}$	1/2	127.987	
92	$7p_{3/2}$	3/2	128.029	
93	$7f_{5/2}$	5/2	131.567	132.647
94	$7f_{7/2}$	7/2	131.568	132.667
95	$8p_{1/2}$	1/2	133.234	
96	$8p_{3/2}$	3/2	133.272	
97	$8f_{5/2}$	5/2	135.977	
98	$8f_{7/2}$	7/2	135.978	
99	$9p_{1/2}$	1/2	136.993	
100	$9p_{3/2}$	3/2	137.019	
101	$9f_{5/2}$	5/2	138.892	
102	$9f_{7/2}$	7/2	138.893	

For Fe IX, atomic data similar to those of Fe VIII are obtained for the configurations of $3s^23p^6$, $3s3p^63d$, and $3s^23p^5nl$ (n=4, 5, 6, 7; l=0, 1,2 and 3). To save space, the complete data sets are not given here. All data are available electronically from http://www.astronomy.Csdb.cn/Eie/.

3. Simulations and analyses of emission spectra of laboratory and astrophysical plasmas

The effective collision strength can be obtained by integrating the collision strength over a Maxwellian distribution

$$\Upsilon_{ij} = \int_0^\infty \Omega_{ij}\exp(-\frac{E}{kT_e})\mathrm{d}(\frac{E}{kT_e}), \qquad (3)$$

where E is the scattered electron energy, k is Boltzmann's constant, and T_e is the electron temperature. The excitation rate coefficients (in units of $\mathrm{cm^3{\cdot}s^{-1}}$) can be obtained from the effective collision strengths

$$C_{ij} = \frac{8.63\times10^{-6}}{g_i T_\mathrm{e}^{1/2}}\mathrm{e}^{-E_{ij}/kT_e}\,\Upsilon_{ij}, \qquad (4)$$

where E_{ij} is the difference in energy between levels i and j, and g_i is the statistical weight of level i. The de-excitation rate coefficients are obtained by detailed balance.

The level populations are obtained by solving the set of coupled rate equations

$$N_j\left[\sum_{i<j}A_{ji} + n_\mathrm{e}(\sum_{i<j}C^\mathrm{d}_{ji} + \sum_{i>j}C^\mathrm{e}_{ji})\right] = \sum_{i>j}N_iA_{ij} + n_\mathrm{e}(\sum_{i<j}N_iC^\mathrm{e}_{ij} + \sum_{i>j}N_iC^\mathrm{d}_{ij}), \qquad (5)$$

where the superscripts e and d refer to electron excitation and de-excitation, respectively, N_j is the number density of the level j, and n_e is the electron density. The intensity distribution at radiation of energy $h\nu$ is given by

$$I(h\nu) = \sum_{i<j}N_jA_{ji}S_{ji}(h\nu), \qquad (6)$$

where S_{ji} is the line profile function, which in general should be a Voigt profile. In the present work, the line widths caused by other broadening mechanisms such as natural lifetime and electron impact broadening are much smaller than Doppler broadening, therefore, we can take it as a Gaussian profile.

Figure 1 shows an overview of the emission spectrum of Fe VIII in a wavelength range of 5–250 nm at an electron temperature of 50 eV and an electron density of 5×10^{11} $\mathrm{cm^{-3}}$. Note that logarithmic scale has been used for the relative intensity. The intensity of the strongest line is normalized to unity. Strong emissions occur near 16 nm that corresponds to 3d → 3p transition. The strongest line is caused by the transition of $3p^63d_{5/2} \rightarrow (3p^3_{3/2}(3d^2_{5/2})_4)_{5/2}$ (Nos. 49 and 2 in Table 1). The second strongest emission regions are located in the ranges of 6–14 nm and 60–80 nm. The emission spectra in the former range are recently studied by Lepson *et al*,[2] while lines in the latter range

are recorded by the solar ultraviolet measurements of emitted radiation (SUMER) spectrometer aboard the Solar and Heliospheric Observatory (SOHO).[33] Efforts have been made to identify the observed lines, yet there are still about 20% of the measured spectral lines that have not been identified. Most of the identified lines are due to astrophysically abundant elements with atomic number $Z \leq 18$, few positive identifications of lines belonging to Fe IV, Fe V, Fe VI, Fe VII, Fe VIII, or Fe IX have been carried out. Recently, Ekberg and Feldman [32,34] identified the Fe VIII lines belonging to transitions of the type $3p^6 4p \rightarrow 3p^6 4d$ and $3p^5 3d^2 \rightarrow 3p^6 4d$ and Fe VII lines to the 3d4s → 3d4p and 3d4p → 3d4d.

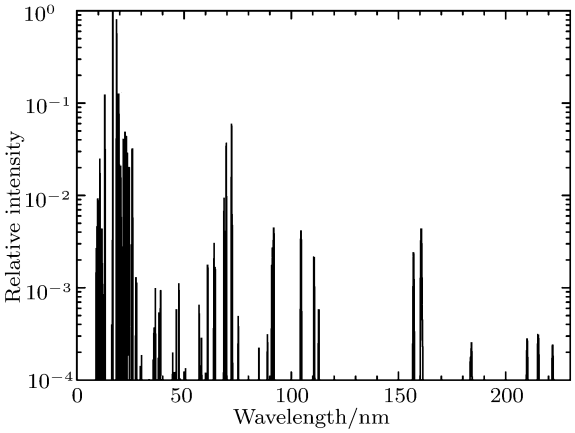


Fig.1. An overview of the emission spectra of Fe VIII in a range of 6–250 nm

First, let us pay attention to the emission spectra in the extreme ultraviolet range of 6–14 nm. Figures 2(a)–(c) show the relative intensities for plasmas at temperatures of 30, 40 and 90 eV and at an electron density of 5×10^{11} cm^{-3}. According to the report of Lepson *et al*,[2] they recorded the emission spectra at an electron density of $\sim5\times10^{11}$ cm^{-3} at the Lawrence Livermore electron beam ion the trap EBIT-II. Figure 2(d) shows their observed spectra. Fairly good agreement is found between the simulated emission lines and the measured ones in the shown wavelength range. In this range, the strongest line originates from the 4f → 3d transition, while other lines from nf → 3d (n=5,6,7,8,9) except those weak ones located at 11–12 nm, which are caused by 4s → 3p transitions.

From the inspection of Figs.2(a)–(c), one can see that the relative intensity ratios of the emission lines are not very sensitive to the temperature. For temperatures of 30, 40 and 90 eV, the ratios vary not too much. Thus it is difficult to infer the plasma temperature in the experiment. Note also that there is a small shift of line position between Figs.2(a)–(c) and Fig.2(d). The wavelengths in Figs.2(a)–(c) are calculated from the difference in energy between the lower and upper levels. For those levels whenever their experimental values are available from the National Institute of Standards and Technology (NIST),[31] we use the experimental results. Fortunately, for these emission lines, the experimental values are available. Therefore, in the experiment of Lepson *et al*,[2] there should be some difference in the alignment of wavelength from other experimental results.

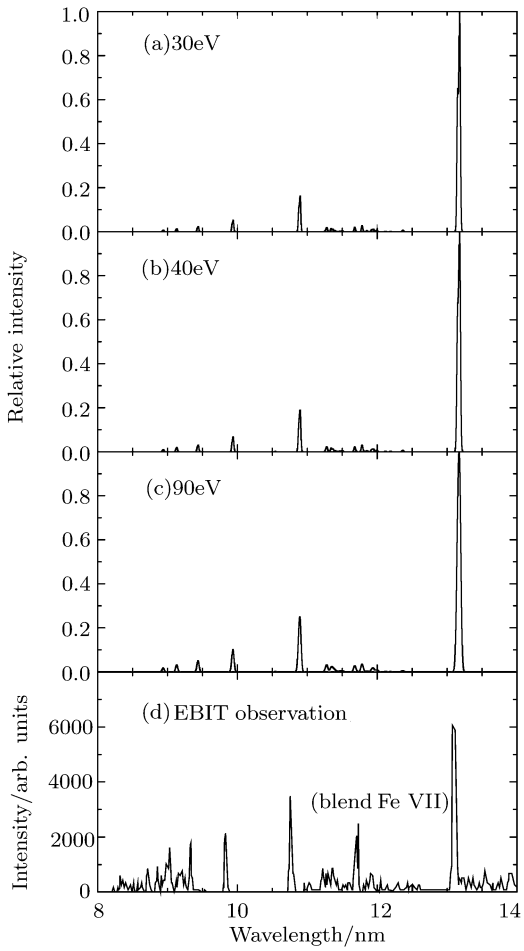


Fig.2. Relative intensity of Fe VIII lines in a range of 8–14nm at temperatures of 30, 40, and 90 eV and an electron density of 5×10^{11} cm^{-3}

Next, let us turn to the wavelength range of 60–78 nm. Figure 3 shows the emission spectra in this range for plasmas at temperatures of 40 and 45 eV. Recently, Ekberg and Feldman [32,34] identified a few Fe VIII lines of transitions $3p^6 4p \rightarrow 3p^6 4d$ and $3p^5 3d^2 \rightarrow 3p^6 4d$ in the SUMER quiet-Sun (QS) spectra in this wavelength range. The identified lines and recorded intensities in the QS are given in Table 2. It shows that the strongest line originates from $3p^6 4p_{3/2} \rightarrow 3p^6 4d_{5/2}$ (No.2) in this wavelength

range. We normalize its intensity to unity and the intensities of other lines relative to the intensity of this line are given. Good agreement is found between our predicted intensities and observations except for lines of $3p^5 3d^2(^1D)^2P^0_{3/2} \rightarrow 3p^6 4d^2 D_{5/2}$ (No.4) and $3p^5 3d^2(^1D)^2P^0_{1/2} \rightarrow 3p^6 4d^2 D_{3/2}$ (No.6). These lines originate from excitation of one electron and de-excitation of another electron. For these two lines, the predicted intensities are smaller than the observations. Part of the reason may be that the observed lines are blended with lines emitted by other ions. If the other ions besides Fe VIII have contributions around this wavelength, then the observed intensity will surely be larger than the intensity caused by Fe VIII alone. Whether this holds true needs to be further studied. On the other hand, the large difference between the observed and theoretical intensities of line No.4 might be partly due to the theoretical uncertainty. Because of the complexity of atomic structure of Fe VIII, we have to omit some configuration interaction. The additional configuration interaction may have contribution to line 4. As we[35] have shown recently, $3p^2 - 3d^2$ and $3p^3 - 3d^3$ core-valence electron correlations are important in calculating the oscillator strengths, and hence the collision strengths. If these electron correlations are included, better agreement might be obtained. From the inspection of Table 2, more Fe VIII lines could be identified in the SUMER spectra, although they are relatively weak. Nonetheless, the lines 7–15 have not been identified yet so far. Some of them are even stronger than lines 5 and 6, which have been identified. Among the unidentified lines, the wavelengths of lines 11 and 12 are accurate, because experimental energy levels exist for the two lines. The wavelengths of other unidentified lines are obtained from theoretical values.

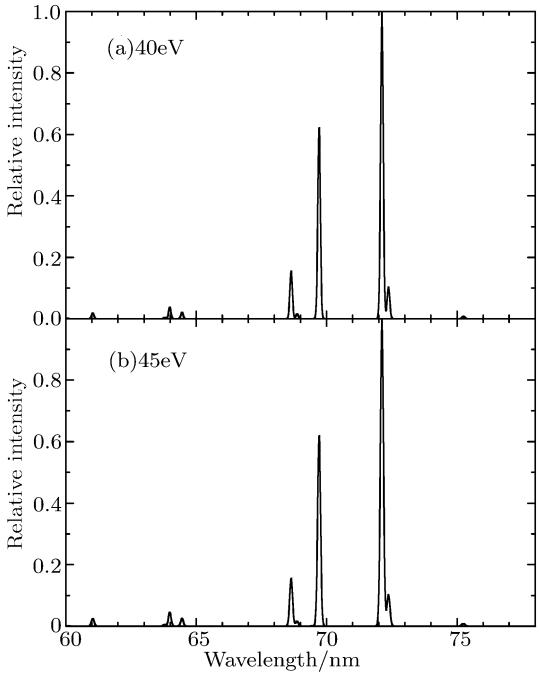


Fig.3. Relative intensities of Fe VIII lines in a range of 60–75nm at temperatures of 40 and 45 eV and an electron density of 5×10^{11} cm^{-3}

Table 2. Wavelength λ and intensity of Fe VIII lines in a range of 60–105 nm. QS refers to quiet-Sun

				Rel. Int.	
No.	Transition	λ/nm	QS Int.[32]	QS	This work
1	$3p^6 4p\ ^2P_{1/2}$-$3p^6 4d\ ^2D_{3/2}$	69.7155	3200	0.842	0.639
2	$3p^6 4p\ ^2P_{3/2}$-$3p^6 4d\ ^2D_{5/2}$	72.1268	3800	1.000	1.000
3	$3p^6 4p\ ^2P_{3/2}$-$3p^6 4d\ ^2D_{3/2}$	72.3742	500	0.132	0.121
4	$3p^5 3d^2(^1D)\ ^2P_{3/2}$-$3p^6 4d\ ^2D_{5/2}$	68.6436	1700	0.447	0.168
5	$3p^5 3d^2(^1D)\ ^2P_{3/2}$-$3p^6 4d\ ^2D_{3/2}$	68.8715	100	0.026	0.021
6	$3p^5 3d^2(^1D)\ ^2P_{1/2}$-$3p^6 4d\ ^2D_{3/2}$	75.2491	100	0.026	0.011
7	$3p^6 4f\ ^2F_{5/2}$-$3p^6 5g\ ^2G_{7/2}$	61.0177			0.021
8	$3p^6 4f\ ^2F_{7/2}$-$3p^6 5g\ ^2G_{9/2}$	61.0509			0.015
9	$3p^6 4d\ ^2D_{3/2}$-$3p^6 5p\ ^2P_{1/2}$	63.9883			0.056
10	$3p^6 4d\ ^2D_{5/2}$-$3p^6 5p\ ^2P_{3/2}$	64.4591			0.035
11	$3p^6 4d\ ^2D_{3/2}$-$3p^6 4f\ ^2F_{5/2}$	90.9254			0.031
12	$3p^6 4d\ ^2D_{5/2}$-$3p^6 4f\ ^2F_{7/2}$	91.2439			0.035
13	$3p^6 4f\ ^2F_{7/2}$-$3p^6 5d\ ^2D_{5/2}$	91.7796			0.040
14	$3p^6 4f\ ^2F_{5/2}$-$3p^6 5d\ ^2D_{3/2}$	91.8593			0.025
15	$3p^6 4s\ ^2S_{1/2}$-$3p^6 4p\ ^2P_{3/2}$	104.5256			0.052

Figures 4(a–c) show the relative intensities of Fe IX lines at temperatures of 25, 30 and 40 eV in a wavelength range of 6–14 nm.One can see that the dependences of intensity ratios of Fe IX lines on temperature are quite different from those of Fe VIII lines. For Fe VIII, the ratios are insensitive to temperature, while for Fe IX, the ratios are very sensitive to temperature.

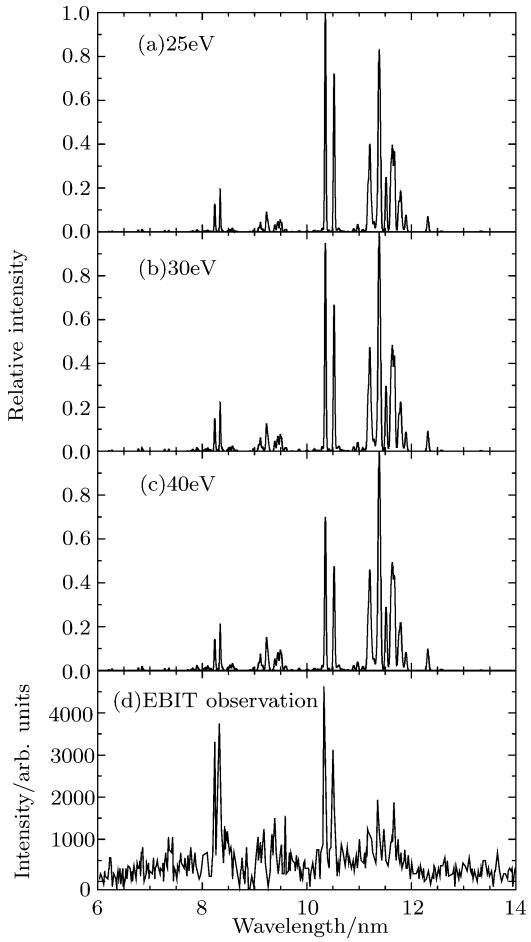


Fig.4. Emission lines of Fe IX in a range of 6–14nm at temperatures of 25, 30, and 40 eV

At a temperature of 25 eV, the strongest line stems from the 4s → 3p transition at a wavelength of 10.357 nm. When the temperature increases to 30 eV, the strongest line changes to a 4f → 3d transition at 11.380 nm and it becomes even stronger as the temperature increases to 40 eV. The sensitivity to temperature of the emission lines shows that we can obtain the information of temperature in the experiment. From the comparison between the observed and simulated spectra, we can deduce that the temperature should be less than 25 eV. However, the intensity ratios between the line at 8.243 nm and the strongest line and between the line at 8.346 nm and the strongest line are basically the same for the three temperatures. When comparing with the EBIT observation (Fig.4(d)) carried out by Lepson *et al*,[2] we find that the predicted relative intensities agree well with the measurements for some lines, while they do not agree so well for some other lines, which can be seen from Table 3. This table shows a comparison between the theoretical and experimental intensities of Fe IX in a range of 6–14 nm at a temperature of 25 eV. The theoretical intensity is normalized to 20 for the line at 10.357 nm, which is the strongest line in this range. The predicted intensities for lines at 11.210 and 10.525 nm are 6 and 14, respectively, which agree well with corresponding observed values of 7 and 15. Yet the difference exists for some other lines. We suggest that the difference might be caused by the blending of lines due to the limited resolution power of the experimental instrument, because some strong lines predicted by theory, for examples, the strong lines at wavelengths of 11.614, 11.411, 11.402 nm, etc, are not found in the experiment.

Table 3. Comparison between the theoretical and experimental relative intensities of Fe IX in a wavelength range of 6–14 nm. The theoretical intensity is normalized to 20 for the line with a wavelength of 10.357 nm

Wavelength λ/nm		Rel. Int.		Wavelength λ/nm		Rel. Int.	
Theo.	NIST	Theo.	Expt.	Theo.	NIST	Theo.	Expt.
142.81		1		114.28	11.380	12	18
140.02		1		113.98	11.353	1	
123.19		1		112.78	11.238	1	
120.01	11.898	1	6	112.40	11.210	6	7
118.45	11.763	1	6	112.09	11.179	2	6
117.97		2		111.99	11.171	1	
117.76	11.680	6	8	105.55	10.525	14	15
117.32	11.642	5	10	103.80	10.357	20	20
116.92	11.521	4	10	94.56		1	
116.37	11.614	3		92.32		1	
116.07		1		91.17		1	
114.59	11.411	3		83.45		3	7
114.55	11.402	6		82.46	8.243	2	7

The wavelengths of these lines are taken from NIST,[31] therefore they should be accurate. If we note that the line at 11.402 nm is located very near that of 11.380 nm, we might suspect that these two lines are not resolved in the experiment. Then the sum of intensities of the two lines is 18, which is in agreement with the experimental value of 18.

4. Conclusions

A complete atomic dataset has been produced for the analysis of emission lines of Fe VIII and Fe IX in both laboratory and astrophysical plasmas. Simulations have been carried out in two wavelength ranges of 6–14 nm and 60–80 nm. The lines in the former range are experimentally studied recently, while the lines concerning emission lines in the latter range are recorded in the SUMER spectra. In the 6–14 nm range, the predicted relative intensities agree well with the measurements for Fe VIII, though the difference exists for Fe IX because of the blending of lines. Much better agreement can be obtained when the blending of Fe IX lines is considered. In the 60–80 nm range, more lines should have appeared in the SUMER spectra for Fe VIII than those identified recently.

References

[1] Hummer D G, Berrington K A, Eissner W, Pradhan A K, Saraph H E and Tully J A 1993 *Astron. & Astrophys.* **279** 298

[2] Lepson J K, Beiersdorfer P, Brown G V, Liedahl D A, Utter S B, Brickhouse N S, Dupree A K, Kaastra J S and Mewe S M 2002 *Astrophys. J.* **578** 648

[3] Sako M, Kahn S M, Behar E, Kaastra J S, Brinkman A C, Boller Th, Puchnarewicz E M, Straling R, Liedahl D A, Clavel J and Santos-Lleo M 2001 *Astron. & Astrophys.* **365** L168

[4] Blustin A J, Branduardi-Raymon G, Behar E, Kaastra J S, Kahn S M, Page M J, Sako M and Steenbrugge K C 2002 *Astron. & Astrophys.* **392** 453

[5] Steenbrugge K C, Kaastra J S, de Vries and Edelson R 2003 *Astron. & Astrophys.* **402** 477

[6] Dai C J and Cheng Z D 2001 *Chin. Phys.* **10** 403

[7] Li C Q, Dai C J and Lu J 2000 *Chin. Phys.* **9** 500

[8] Liu Y B, Pang W N, Ding H B and Shang R C 2005 *Acta Phys. Sin.* **54** 5121

[9] Jin S Q and Xu Z Z 1998 *Acta Phys. Sin.* **47** 577

[10] Czyak S J and Krueger T K 1966 *Astrophys. J.* **144** 381

[11] Blaha M 1969 *Astrophys. J.* **157** 473

[12] Pindzola M S, Griffin D C and Bottcher C 1989 *Phys. Rev.* A **39** 2385

[13] Saraph H E, Storey P J and Taylor K T 1992 *J. Phys.* B **25** 4409

[14] Lynas-Gray A E, Seaton M J and Storey P J 1995 *J. Phys.* B **28** 2817

[15] Seaton M J 1987 *J. Phys.* B **20** 6363

[16] Tiwary S N 1982 *Chem. Phys. Lett.* **93** 47

[17] Tiwary S N 1983 *Astrophys. J.* **269** 803

[18] Tiwary S N, Kumar P and Roy R P 1996 *Pramana* **46** 381

[19] Hibbert A 1975 *Comput. Phys. Commun.* **9** 141

[20] Fischer C F 1991 *Comput. Phys. Commun.* **64** 369

[21] Fawcett B C 1989 *At. Data Nucl. Data Tables* **43** 71

[22] Bhatia A K and Eissner W 2000 *At. Data Nucl. Data Tables* **76** 270

[23] Eissner W, Jones M and Nussbaumer H 1972 *Comput. Phys. Commun.* **8** 270

[24] Griffin D C, Pindzola M S and Badnell N R 2000 *Astron. & Astrophys. Suppl. Ser.* **142** 317

[25] Storey P J, Zeippen C J and Le Dourneuf M 2002 *Astron. &Astrophys.* **394** 753

[26] Flower D R 1977 *Astron. & Astrophys.* **56** 451

[27] Haug E 1979 *Astrophys. J.* **228** 903

[28] Fawcett B C and Manson H E 1991 *At. Data Nucl. Data Tables* **47** 17

[29] Gu M F 2002 *Astrophys. J.* **579** L103

[30] Burgess A and Sheorey V B 1974 *J. Phys.* B **7** 2403

[31] See NIST Atomic Spectra Data Base, http://physics.nist.gov/cgi-bin/AtData/main_asd

[32] Ekberg J O and Feldman U 2003 *Astrophys. J.* **595** 517

[33] Feldman U, Behring W E, Curdt W, Schuhle U, Wilhelm K, Lemaire P and Moran T M 1997 *Astrophys. J. Suppl. Series* **113** 195

[34] Ekberg J O and Feldman U 2003 *Astrophys. J. Suppl. Series* **148** 567

[35] Zeng J L, Jin F T, Zhao G and Yuan J M 2003 *J. Phys.* B **36** 3457